Adsorptive remediation of cobalt oxide nanoparticles by magnetized α-cellulose fibers from waste paper biomass

Avinash Kadam, Rijuta Ganesh Saratale, Surendra Shinde, Jiwook Yang, Kyojung Hwang, Bhupendra Mistry, Ganesh Dattatraya Saratale, Saifullah Lone, Dae-Youg Kim, Jung-Suk Sung, Gajanan Ghodake

PII: S0960-8524(18)31574-8
DOI: https://doi.org/10.1016/j.biortech.2018.11.041
Reference: BITE 20693

To appear in: *Bioresource Technology*

Received Date: 8 October 2018
Revised Date: 6 November 2018
Accepted Date: 11 November 2018

Please cite this article as: Kadam, A., Saratale, R.G., Shinde, S., Yang, J., Hwang, K., Mistry, B., Saratale, G.D., Lone, S., Kim, D-Y., Sung, J-S., Ghodake, G., Adsorptive remediation of cobalt oxide nanoparticles by magnetized α-cellulose fibers from waste paper biomass, *Bioresource Technology* (2018), doi: https://doi.org/10.1016/j.biortech.2018.11.041

Adsorptive remediation of cobalt oxide nanoparticles by magnetized α-cellulose fibers from waste paper biomass

Avinash Kadam[a], Rijuta Ganesh Saratale[a], Surendra Shinde[b], Jiwook Yang[b], Kyojung Hwang[b], Bhupendra Mistry[c], Ganesh Dattatraya Saratale[c], Saifullah Lone[d], Dae-Youg Kim[b], Jung-Suk Sung[e], and Gajanan Ghodake[b]*

[a]Research Institute of Biotechnology & Medical Converged Science, Dongguk University-Seoul, 32, Dongguk-ro, Ilsandong-gu, Goyang-si, Gyonggido 10326, Republic of Korea

[b]Department of Biological and Environmental Science, College of Life Science and Biotechnology, Dongguk University-Seoul, 32, Dongguk-ro, Ilsandong-gu, Goyang-si, Gyonggido 10326, Republic of Korea

[c]Department of Food Science, College of Life Science and Biotechnology, Dongguk University-Seoul, 32, Dongguk-ro, Ilsandong-gu, Goyang-si, Gyonggido 10326, Republic of Korea

[d]Cogno-Mechatronics Engineering, Department of Optics and Mechatronics Engineering, College of Nanoscience and Nanotechnology, Pusan National University, Busan 46241, Republic of Korea

[e]Department of Life Science, College of Life Science and Biotechnology, Dongguk University-Seoul, 32, Dongguk-ro, Ilsandong-gu, Goyang-si, Gyonggido 10326, Republic of Korea

Corresponding author:

*Gajanan Ghodake

Tel: +82-31-961-5159

Fax: +82-31-961-5122

Email: ghodakegs@gmail.com

Abstract

Remediation of engineered-nanomaterials is an up-coming major environmental concern. This study demonstrates adsorptive-remediation of cobalt oxide nanoparticles (CoO NPs) from the water. The α-cellulose-fibers were extracted from waste-paper biomass (WP-αCFs) and magnetized with Fe_3O_4 NPs (M-WP-αCFs). The XRD, FT-IR, and TGA were performed for detailed characterization of the newly developed bioadsorbent. The M-WP-αCFs was then applied for adsorptive remediation of CoO NPs. The adsorptive kinetics of CoO NPs adsorption onto the M-WP-αCFs reveals the pseudo-second-order model. The various adsorption isotherm studies revealed Langmuir is a best-fit isotherm. A prominently high adsorption capacity q_m (1567 mg/g) corroborated extraordinary adsorptive potential of M-WP-αCFs. Furthermore, CoO NPs were adsorbed onto M-WP-αCFs were analyzed by the XPS, VSM, and TEM. Therefore, this study gave rise WP biomass extracted and rapidly-separable nano-biocomposite of 'M-WP-αCFs' with a high-capacity for CoO NPs remediation, and can be further applied in remediation of several other engineered-nanomaterials.

Keywords: Sludge free remediation, engineered nanomaterials; cobalt oxide, paper waste, α-cellulose-fibers; Fe_3O_4 NPs

1. Introduction

Water is critically essential for sustaining life on earth. However, the quantity of the water, is declining at an alarming speed and magnitude in both developed and emerging nations. The concept of flowing pristine water bodies that once could impart psychological and economic richness to mankind, also remained healthy habitat to thousands of imperiled aquatic species is fading away quickly. The imbalance between needs and wants of overpopulation, unregulated industrialization, and uneducated agricultural activities has poisoned the water bodies of Earth beyond repair (Wagner et al., 2014). In recent years, the rapid increase in production of engineered nanoparticles (ENPs) with the arrival of nanotechnology resulted into enormous applications of nanomaterials in the form of various products or manufacturing as a process enhancers (Hutchison, 2016). Although, nanotechnology has gripped the imagination of academic and industrial innovators of this age with practical and futuristic applications; nonetheless, the subject has also spilled enormously practical ecological problems. The ENMs are being released into the environment through different ways, which are emerging as severe pollutants to air, water, and soil (Balmuri et al., 2017). Consequently, this menace has created a demand for the removal of such particulate matter from the ecosystem in general, but from water in particular. Recently, it has been speculated that the rheological properties of sludge are likely to be affected by NPs; however, little information is so far available about the behaviors of sludge in such conditions (You et al., 2018). Reijnder (Reijnders, 2006) suggested that most of the standard wastewater treatments are poorly suited to remove a range of NMs, it was also reinforced by (Wiesner et al., 2006), in regards to the current water treatment processes. In particular, interest in the effective removal of nanomaterials from wastewater thus could avoid the dispersions of NPs and contamination into the aquatic environment (Nowack & Bucheli,

2007). On the other hand, increasing use of ENMs in industrial processes and wastewater treatment plants will very likely lead to the discharge of such materials and cause adverse effects into the environment (Nowack & Bucheli, 2007).

The CoO NPs and their alloys are well-known catalysts for water oxidation, and also be used for modification of wide-band-gap of oxide semiconductors (Kazuhiko et al., 2016). Thus, NPs may enter into aquatic environment directly from the disposal of wastewater effluent, or indirectly from soils (Batley et al., 2013). However, little information is available about the pH influence, the behavior of cobalt, and biomolecules in the aqueous environment. Therefore, it is vital to discover the possible risks related to the specific NPs in the environment. The urinary cobalt concentrations were found to be highest in African copper belt population, thus monitoring of metal exposure, pathways of exposure, and health significance is not clear (Banza et al., 2009). Possible toxic effects of soluble oxide NMs on plant species, such as CoO NPs, have been recently investigated on *Allium ceca* (onion), (Ghodake et al., 2011) and *Glycine max* (soybean) (Quoc Buu et al., 2014). Faisal et al (Faisal et al., 2016), investigated DNA damage and cell death in *Solanum melongena* (eggplant) after exposure to CoO NPs via mitochondrial swelling and enhanced no signaling pathway. These studies demonstrate a strong need for effective removal of CoO NPs and the prevention of oxide NPs into the aquatic environment.

Cellulose is the most abundant biopolymer on the earth, is also being extensively recycled (Gomes et al., 2018). The valorization, co-pyrolysis, anaerobic digestion, and recycling can save landfill spaces and reduce the need for incineration of waste-paper biomass (WP), thus producing value-added products with fever chances of air pollution (Fang et al., 2018). Every ton of recycled cellulose saves an average of 17 to 18 large trees plus energy related to pulping,

processing and finishing (Bajpai, 2014). In addition to this, αCFs, including abundant O-donating/ binding sites in its structure has made this material more viable for environmental-related applications, and has been extensively utilized as a bioadsorbent material for metal ions, dyes, pesticides and micro-pollutants (Cai et al., 2017; Singh & Ambika, 2018). In addition to this, an emerging area that could lead in future such as selective adsorption, aerobic oxidation, designing electrochemical devices, reformation nano- and meso-porous materials (Chen et al., 2014; Dutta et al., 2017; Nguyen et al., 2016; Shieh et al., 2013). In previous reports, immobilization of laccase, catalase, and many other enzymes were demonstrated by combining enzymes with metal-organic frameworks, alginic acid, and cellulose fibers to enhance the stability and recyclability of enzymes (Ghodake et al., 2018; Shieh et al., 2015). A αCFs has been extensively used in various industries of textiles, printing, dyeing, exploration, food, lithium-ion batteries, ceramics, and pharmacy because of their environmental friendliness, lightweight, low cost, and biodegradability (Nechyporchuk et al., 2017). Inspired by the superb adsorption ability of the cellulose, the biocompatibility, and the ease of separating magnetic NPs, here, this study present WP-αCFs coated by Fe_3O_4 NPs in the removal of CoO NPs from aqueous solutions.

In the current work, the nanocomposites (Fe_3O_4 magnetite into α-celluloses matrices) provides excellent mechanical, physical and chemical properties. As an exemplary nanomaterial, this study chose an industrially important CoO NPs previously used in numerous important toxicity studies. The potential use of M-WP-αCFs is identified as an efficient bioadsorbents for CoO NPs and a useful tool for ease of separation. The adsorptive isotherm models were investigated to elucidate the phenomenon of adsorption. Finally, after adsorption of CoO NPs on

M-WP-αCFs, detailed characterization techniques such as XPS, VSM, and TEM were deployed to rationalize the CoO NPs removal process. Obviously, the prepared M-WP-αCFs as novel supports for CoO NPs is promising and competitive for sludge free remediation practices.

2. Materials and methods

2.1. Chemicals

$FeCl_3 \cdot 6H_2O$, $FeCl_2 \cdot 4H_2O$, and $NH_3 \cdot H_2O$ were obtained from Daejung chemicals, South Korea. Pure cobalt (II, III) oxide (CoO NPs) having diameters of approximately 50 nm were purchased from Sigma Aldrich Chemicals. The CoO NPs in DI water were dispersed by sonication and used freshly in adsorption studies.

2.2. Preparation of recycled *WP-αCFs*

This study aims to extract the αCFs from WP as a high-yield cellulosic source. Typically, 10 g WP was soaked in alkali water for 12 h, and sonicated in an ultrasonic bath for 2 h at 30 °C. The white pulp sample was again treated with NaOH (17.5%, w/v) at 30 °C for 6 h to remove mannan, xylan, and lignin, and residual resin content, without losing of αCFs (Ghodake et al., 2018). The α-cellulose is long-chain cellulose, insoluble in NaOH solution (17 to 20%) (Phinichka & Kaenthong, 2018). The treated solution was filtered and pressed to remove excess NaOH, and rinsed the white pulp with DI water. Then, 1% (w/v) hydrochloric acid was used to treat alkali pulp. Finally, a large volume of cold DI water was flushed until the washings reached neutral pH value (Loader et al., 1997). The yield of α-cellulose was found about 59%; thus, generation of the αCFs from WP is facile, reproducible, and cost-effective. Lastly, a floppy

white powder of WP-αCFs was dried using the lyophilizer (Ilshin Biobase FD-8508). It is well known that higher the α-cellulose level better the quality of the bio-adsorbent and value-added products manufactured (Takagi et al., 2013).

2.3. Preparation of M-WP-αCFs

The preparation of WP-αCFs loaded with Fe_3O_4 was performed according to the previous report (Ghodake et al., 2018). Typically, dry powder of WP-αCFs (3 g) was dissolved in DI water (500 mL) and kept in bath sonication for 2 h (Power Sonics-520). The stock solution of $FeCl_3.6H_2O$ and $FeCl_2.4H_2O$ (ratio, 2:1) were prepared separately and allowed to dissolve on the magnetic stirrer. The WP-αCFs solution moved to the clean and dry beaker (1000 mL) and allowed to reach 60 °C condition under shaking conditions. At this time, $FeCl_3.6H_2O$ was added drop-wise and then $FeCl_2.4H_2O$ in the presence of nitrogen gas. 40 mL ammonia solution (25 %) added drop-wise to form crystalline Fe_3O_4 NPs onto the WP-αCFs surfaces. The black colored co-precipitate was refluxed for next 15 min at 60 °C. The synthesized M-WP-αCFs nanocomposite was washed thoroughly with the help of the external magnetic field, and the pure M-WP-αCFs was freeze-dried using the lyophilizer (Ilshin Biobase FD-8508). The freeze dried M-WP-αCFs was powdered and applied for adsorptive removal of CoO NPs.

2.4. Adsorption studies

To study the adsorption kinetics, CoO NPs (100 $mg.L^{-1}$) and M-WP-αCFs (100 $mg.L^{-1}$) was taken into the 50 mL of distilled water. The mixture was shaken at 200 rpm. The 2 ml sample was removed after 1, 3, 6, 9, 12, 24, 48, and 72 h. The M-WP-αCFs was removed magnetically and retained supernatant was analyzed by UV-vis spectroscopy. Further, the

adsorption isotherm was studied by taking increasing concentrations of the CoO NPs (25, 50, 100, 150, 200, 250, 300, 350, and 400 mg.L^{-1}) and M-WP-αCFs (100 mg.L^{-1}) in 10 ml of distilled water. The samples were shaken for 200 rpm for 48 h and residual concentrations of CoO NPs were measured spectrophotometrically. Effect of pH on adsorption of CoO NPs was determined in the range 4 to 9 for 12 h at 200 rpm and ambient temperature (22 °C). The quantitative adsorption of CoO NPs q_e (mg·g^{-1}) by M-WP-αCFs were calculated by using the following equation (1).

$$q_e = \frac{(C_0 - C_e)\mathrm{V}}{W} \quad (1)$$

Where, C_0 (mg·L^{-1}) is the initial concentration of CoO NPs; C_e (mg·L^{-1}) is the residual concentration of the CoO NPs after removal; V is the volume of CoO NPs solution in L; W is the number of M-WP-αCFs in g.

2.5 Structural characterizations

The vibrating sample magnetometer (VSM) model Lakeshore, Model: 7407 was used to record the hysteresis magnetization curve of M-WP-αCFs. The thermogravimetric analyzer (TGA) was used to reveal thermal properties of WP-αCFs and M-WP-αCFs, typically ~5 mg dry sample was characterized with a TA Instruments Q-600 in temperature range (25–800 °C) and under steady nitrogen gas flow ~245 mL/min with heating rate (10 °C/min). X-ray diffraction (XRD) spectra of M-WP-αCFs was acquired using XRD model Ricaku Ultima IV provided with Cu Kα radiation (λ = 1.5418 Å). The XRD spectrum was noted in steps of 0.045° at a count time of 0.5 s in the range of 2θ from 10-90°. Fourier-transform infrared spectroscopy (FT-IR) studies

of WP-αCFs and M-WP-αCFs samples were performed using IR spectrometer (Thermo Electron Nicolet 6700) after preparing and drying KBR pellets, FT-IR spectrum was scanned from 500-4000 cm^{-1} with a resolution of 5 cm^{-1} for 5 scans. Tecnai-G^2 transmission electron microscope (TEM) was used for imaging, energy dispersive X-ray spectroscopy (EDS) and selected area by electron diffraction (SAED) pattern. TEM analysis of M-WP-αCFs was performed before and after remediation experiments using carbon-coated copper grids (300 mesh).

3. Results and Discussion

3.1. Recycling and magnetization of WP-αCFs

Cellulose is a renewable biopolymer on the earth and it is mainly used to produce paper, napkins, cardstocks, and paperboard. Cellulose is abundantly available but important commercial raw materials and is mainly received from wood pulp and cotton fibers for manufacturing and practical use. Along with cellulose, WP contains a variety of inorganic and organic ingredients, various chemicals as phthalates, phenols, mineral oils, polychlorinated biphenyls (PCBs) and toxic metals, which can pollute the newly made paper products (Pivnenko et al., 2015). The paper industry waste, used WP is generally discarded in to waste site landfills, and cremation of waste-disposal leads us to wider questions about waste management and air pollution. WP can be recycled as briquettes for domestic and commercial use, like biochar briquettes or other common fuels (Xiu et al., 2018). Such as, proposals for recycling and converting cellulose into biofuels such ethanol is also under serious investigation to use as an alternative fuel. The demand for recycled or processed cellulose is constantly rising to address the WP problem and produce cellulose-based commercial and composite products. The αCFs have revealed for their great potential for improving mechanical and physical properties in biopolymer-based nanocomposites

(Rotaru et al., 2018). High cellulose content in the WP is promising to extract αCFs and use for preparing biopolymer-based nanocomposites for various environmental applications related to adsorption and catalysis of pollutants (You et al., 2018; Zare et al., 2018).

In this study, the WP reprocessed to form pure αCFs with a high-yield using combined mechanical and chemical treatments. Briefly, recycled WP pulp was prepared using blending, and sonication treatment, finally cleansed with sodium hydroxide treatment. The alkali treatment allowed to extract discrete αCFs from the matrixes of WP and to dissolve noncellulosic materials. This way, WP was successfully recycled to isolate α-CFs with a yield of about 59% (w/w). The carbohydrate portion of cellulose-containing materials does not dissolve in a sodium hydroxide (17.5%) solution at 20-30 °C is α-cellulose, which is a major constituent as compared to the β cellulose and γ cellulose. The use of ultrasonic cavitation combined with NaOH treatments found to be useful in improving the physical properties of recycled α-CFs through an increase in the surface area (Xiuyan et al., 2015). SEM images revealed the surface morphology of the α-CFs, the cylindrical structure consisting of stacked fibers having a size in the range of micrometer can be observed (see the supplementary materials). In one of the previous report, it was recommended that the WP fibers are the purest form of cellulosic materials for extraction of α-CFs with a yield of more than 60% wt/w (Ghodake et al., 2018). In further experiments, the white colored floppy powders of α-CFs derived from WP were found to be insoluble in DI water and shown usability in preparing Fe_3O_4 NPs based nanocomposites and applying in remediation of CoO NPs. Herein, WP extracted αCFs was established as a raw material to fabricate M-WP-αCFs a potential bio-adsorbents. This reports finally describes the role M-WP-αCFs in high-concentration remediation of CoO NPs from the water. The details of the report, adsorption

kinetics of CoO NPs and detailed characterization of the final nanoproduct, labelled as M-WP-αCF-CoO NPs are described and also illustrated in a graphical abstract.

3.2. Characterization of M-WP-αCFs

Pure cellulose consists of three kinds of atoms, oxygen, carbon, and hydrogen, which forms a straight-chain biopolymer having six-membered glucose rings with OH groups. FT-IR analysis of the samples was shown in the supplementary materials. Many of the FT-IR bands corresponds to WP-αCFs and M-WP-αCFs was identified, including 3371, 2917, 1430, 1375, 1161, 1053, and 897 cm^{-1}. FT-IR absorptions arise typically from nanocellulosic materials, lignin, and other contaminants were certainly not seen due to the high purity of the regenerated αCFs. Characteristic FT-IR bands of cellulose have been identified for OH stretching vibrations at 3371 cm^{-1}. The characteristic FT-IR bands of cellulose observed in the region 3600-3200 cm^{-1} is owed to the OH stretching frequencies of the cellulose. The 1375 cm^{-1} band is accountable to C−H bending vibrations, and it may also be suitable for identifying crystallinity of cellulose in ratio with the help of 2917 cm^{-1} band identified for asymmetric CH_2 stretching vibrations. Alternatively, the vibration peak at 1430 cm^{-1} has been acknowledged as a "crystallinity" absorption band, and its ratio with the 897 cm^{-1} vibration band also used to calculate crystallinity index of cellulose (Park et al., 2010). The 1161 cm^{-1} band is attributed to anti-symmetrical bridge C−O−C stretching vibrations, particularly from WP-αCFs. The 1018 and 1053 cm^{-1} band is recognized for C−O stretching vibration mode, and 1056 existed as a sharp peak in the FT-IR spectra of WP-αCFs (Abidi et al., 2014).

XRD analysis of the M-WP-αCFs was shown in the supplementary materials. The XRD of M-WP-αCFs exhibits five peaks that agree with the known reflex positions of magnetite (2θ =

31.1, 37.5, 45.0, 59.4, and 65.5 °) due to the 220, 311, 400, 511, and 440 lattice planes, respectively, (JCPDS#19–0629). From the XRD patterns, characteristic peaks are in good agreement with the face-centered cubic lattice structure of the Fe_3O_4. XRD results observed for M-WP-αCFs was similar to those reported in the literature (Silva et al., 2013). The XRD of M-WP-αCFs shows the same peaks as shown for those of uncoated Fe_3O_4 NPs, indicating that the surface coating by WP-αCFs does not affect the crystallinity of the core magnetite. The XRD measurements of bare and polyethylene glycol-coated Fe_3O_4 NPs used to identify the crystal phases, all the major peaks shown in the XRD pattern were identical to Fe_3O_4 NPs present onto the M-WP-αCFs (Mukhopadhyay et al., 2012).

TGA curves of WP-αCFs and M-WP-αCFs are presented in Fig. 1a. It revealed that M-WP-αCFs were started decay at a lower onset of temperature than that of pure WP-α-CFs. However, M-WP-αCFs had higher stability against temperature, representing forming of more residual mass remained (24%) up to a temperature of 800 °C (Fig. 1a). The Fe_3O_4 loading caused a difference in TGA results, the degree of crystallinity after magnetization of amorphous WP-αCFs was better due to the crystallinity of Fe_3O_4 NPs present onto the surfaces of the M-WP-αCFs. Furthermore, the recycled WP-α-CFs showed initial of weight loss at about 340 °C, which was slightly larger than that of the M-WP-αCFs. Particularly, Fe_3O_4 NPs must be contained in the incremental residual char of M-WP-αCFs, indicating Fe_3O_4 NPs must be deeply implanted in the matrices of the WP-α-CFs. This result syncs with the results mentioned above on the XRD and the ones that will be mentioned below in the description of VSM results. Comparable observation for cellulose, chitosan, and their magnetized cellulose-chitosan nanocomposite was recently reported by (Peng et al., 2014). The weight loss of cellulose in the region 200-350 °C

and 400-500 °C can be referred to the initiation of thermal degradation and complete decomposition of the composite, respectively (Ma et al., 2012).

3.3 Effect of pH on CoO NPs adsorption

The effect of pH values on the remediation of CoO NPs ($mg.L^{-1}$) and adsorptive behavior of M-WP-αCFs was first investigated in the pH range 4 to 9. The effect of the pH on the removal of CoO NPs was executed using 100 mg L^{-1} of M-WP-αCFs (Fig. 1b). The results of the non-treated samples exhibited that varying pH value of the CoO NPs solution had a minor effect on the maximum absorption wavelength and absorbance intensity (data not shown). The acidic pH was less favorable for adsorption of CoO NPs, and the efficiency at pH 4. It was observed that the adsorption of CoO NPs on M-WP-αCFs was started improving from pH 5 to 9 (Fig. 1b). It was seen that the adsorption of CoO NPs onto the M-WP-αCFs can be facilitated in a broad pH range from 5 to 9, make this method more practical and sustainable remediation of CoO NPs contaminated water samples. These results indicate increases the availability of negative charge density present onto the M-WP-αCFs, thus provides adsorption sites, and reinforces interactions among positively charged CoO NPs. On the other hand, M-WP-αCFs in the acidic solution was kept on protonated, and the excessive H^+ ions present onto the M-WP-αCFs hinders adsorption of CoO NPs. However, M-WP-αCFs turn into deprotonated in both neutral and alkaline solution; thus, electrostatic interaction facilitated higher adsorption efficiency for CoO NPs as reported in the recent report (Zhou et al., 2013).

3.4 Adsorption kinetics study

Kinetics of CoO NPs adsorption on the M-WP-αCFs were studied by applying the pseudo-first and second-order kinetic models. The equations of the pseudo-first-order and

second-order-models were expressed as following (Eq. (2)) and (Eq. (3)) (Kadam et al., 2013a; Kadam et al., 2013b).

$$q_t = q_e(1 - e^{-k1t}) \quad (2)$$

$$q_t = \frac{k_2 q_e^{\,2} t}{1 + k_2 q_e t} \quad (3)$$

Where, q_e and q_t are the amount of CoO NPs adsorbed (mg g^{-1}) at equilibrium and at time t (min), respectively, and k_1 is the pseudo-first-order rate constant of adsorption (min^{-1}). While, k_2 (g mg^{-1} min^{-1}) is the second order rate constant. The values of k_1, k_2 and q_{ecal} were calculated from the software OriginPro8. Figure 2 displayed the pseudo-first and second order adsorption kinetics of CoO NPs on M-WP-αCFs. Figure 2 clearly informs that CoO NPs adsorption achieves the equilibrium within 48 h with the equilibrium uptake amount of 573 mg g^{-1}. Table 1 lists the detailed sorption rate constants associated with pseudo-first and second-order kinetics model. The rate constant for pseudo-first-order and second-order, k_1 and k_2, were obtained to be 0.673 and 0.0016, respectively (Table 1). The obtained results revealed that the q_{ecal} value of the pseudo-first-order was not close to the actual q_{exp} value (Table 1). However, the q_{ecal} values of pseudo-second order found to be closer to the q_{exp} value (Table 1). Compared to the first-order kinetic model, the pseudo-second-order kinetic model had a higher correlation coefficient (Table 1), suggesting that the CoO NPs adsorption on M-WP-αCFs is chemisorption rather than the physisorption. Therefore, the closeness of q_{ecal} and q_{exp} value in pseudo-second order with the higher correlation coefficient has corroborated that adsorption of CoO NPs on M-WP-αCFs follows the pseudo-second-order kinetic model, and gave an idea about the chemisorption-based adsorption phenomena.

3.5. Adsorption isotherms study

Equilibrium adsorption isotherm models such as; Langmuir, Freundlich, and Tempkin were investigated for the adsorption of CoO NPs on M-WP-αCFs (Fig. 3(a-c). The isothermal adsorption process mechanism was studied by the non-linear fitting method using software OriginPro8. The Langmuir equation mainly assumes that the adsorption process is monolayer in nature. In comparison, the Freundlich isotherm empirical equation assumes a heterogeneous nature of the system. However, the Tempkin model represents the heat of the adsorption. The non-linear equations of the isotherm models; Langmuir (Eq. 4) (Langmuir, 1916), Freundlich (Eq. 5) (LeVan & Vermeulen, 1981), and Tempkin (Eq. 6) (Guacci et al., 1977), were represented as;

$$q_e = \frac{q_m K_a C_e}{1 + K_a C_e} \tag{4}$$

$$q_e = K_F C_e^{(\frac{1}{n})} \tag{5}$$

$$q_e = \frac{RT}{b_T \ln(A_T C_e)} \tag{6}$$

Where, q_e is the CoO NPs adsorption capacity of the adsorbent at equilibrium (mg/g), C_e is the equilibrium concentration of CoO NPs in solution (mg/L), q_m is the maximum adsorption capacity (mg/g), and K_a, K_F, n, b_T and A_T are the constants of Langmuir, Freundlich, and Tempkin isotherm constants (Eqs. 4-6), respectively. Figure 3 represented the fitting pattern of the Langmuir, Freundlich, and Tempkin isotherms. The Langmuir adsorption found to be closely fit to the experimental data rather than Freundlich, and Tempkin isotherms. Table 2, enlists all

the constants and correlation coefficients (R^2) values of the studied isotherms. The correlation coefficients (R^2) for fitting of the Langmuir ($R^2 = 0.9903$), Freundlich ($R^2 = 0.9773$), and Tempkin ($R^2 = 0.9876$) isotherm models. From these observed R^2 values, it was concluded that the data obtained from the experiments gave fit best to the Langmuir model. As per the obtained R^2 values, adsorption of CoO NPs on the M-WP-αCFs followed the order of the isotherm models as: Langmiur>Tempkin>Freundlich. The maximum adsorption capacity (q_m) was observed to be 1567 mg/g, suggesting the very high capacity of the M-WP-αCFs to adsorb the CoO NPs from the water. The Langmiur adsorption pattern confirms the monolayer nature of the CoO NPs over the surface of the M-WP-αCFs. Figure 3 (d) represents the plot for separation factor (R_L). R_L factor was calculated to assess the favorability of the adsorption process. R_L factor mainly expressed as the following equation (Eq. 7),

$$R_L = \frac{1}{1 + K_a C_o} \tag{7}$$

Where, C_o is the initial CoO NPs concentration, and K_a is the obtained Langmuir isotherm constant. Based on the isotherm data, the R_L values gave an indicator of whether the adsorption process is (i) favorable (R_L<1), (ii) unfavorable (R_L >1), (iii) linear (R_L = 1), or (iv) irreversible (R_L = 0) (Kadam et al., 2016; Kadam & Lee, 2015). The R_L value for adsorption of CoO NPs on M-WP-αCFs was found to be fell in between 0 and 1 (Fig. 3d), corroborating a favorable adsorption dynamics.

3.6 Characterizations of M-WP-αCF-CoO NPs

After establishing the successful adsorption process and adsorption experiments, the CoO NPs adsorbed over the M-WP-αCFs was thoroughly characterized by XPS, VSM and TEM analyze.

Thorough characterization was needed to corroborate and support the obtained high-capacity and significant remediation of CoO NPs from water by M-WP-αCFs.

3.6.1 XPS analysis

Surface elemental analysis of CoO NPs loaded over M-WP-αCFs was carried out by XPS analysis. Supplementary material displays XPS spectrum of WP-α-CFs, M-WP-αCFs, and M-WP-αCF-CoO NPs. High resolution spectrum of C1s, O1s, Fe2p and Co2p from M-WP-αCF-CoO are also shown in the supplementary material. The WP-α-CFs gave binding energies of 284.2 and 532.88 eV of C1s and O1s, respectively. The M-WP-αCFs XPS spectrum showed the binding energies of 284.6, 532.94 and 710.85 eV of C1s, O1s and Fe2p, respectively. However, XPS spectrum of M-WP-αCF-CoO NPs exhibited the binding energies of 284.6, 530.17, 711.20 and 780.33 of C1s, O1s, Fe2p, and Co2p, respectively. Therefore, these obtained results were strongly corroborated a supermagnetic modification made in the WP-αCFs and successful loading of CoO NPs on M-WP-αCFs. The high-resolution spectrum of each peak, C1s, O1s, Fe2p and Co2p from M-WP-αCF-CoO NPs were displayed in supplementary material. The Fe_3O_4 NPs were evidenced by well-characterized $Fe2p_{3/2}$ and $Fe2p_{1/2}$ peaks with the binding energies of 711.90 and 724.60 Ev, respectively (see in the supplementary material). The typical characteristic Co2p peak represents $Co2p_{3/2}$ and $Co2p_{1/2}$ at the binding energies of 780.5 and 795.06 eV, with their respective sattellite peaks (as shown in the supplementary material). The observations revealed a well characterized and sharp Co2p peak and corroborated a highly efficient loading of CoO NPs over the M-WP-αCFs surface. Therefore, the overall XPS analysis confirmed the loading of CoO NPs over the M-WP-αCFs surface.

3.6.2 VSM analysis

The magnetization curve for M-WP-αCFs and M-WP-αCF-CoO NPs as shown in the supplementary material. Fe_3O_4 NPs entrapped onto the surfaces of the WP-αCFs have shown good magnetic response and are readily attracted to a magnet placed apart as shown in the supplementary material. The saturation magnetic moments obtained is about 7.42 emu g^{-1} for M-WP-αCFs, as shown in the supplementary material. As seen in the VSM response, the coercivity and reminisce values of the M-WP-αCFs curve was detected to be zero, this indicating superparamagnetic nature. However, the less saturation magnetic moment values for the CoO NPs adsorbed M-WP-αCFs are found to be 7.21 emu g^{-1}, confimmed successful remediation of CoO NPs from the water. It is well known that magnetization saturation value is either affected by changes in the crystallinity, size, and the composition after use in various applications or loading of bulky material (Kadam et al., 2017; Wahajuddin & Arora, 2012). The obtained results revealed no significant change in magnetic saturation value. Therefore, the magnetic separation potential of the remediated product was successfully retained after the adsorption process. The magnetically modified WP-α-CFs was prepared using a simple co-precipitation technique and was characterized comprehensively. The obtained remediation product showed that CoO NPs adsorbed onto the M-WP-αCFs have relatively high stability at broad pH and temperature range. Adsorption of CoO NPs within M-WP-αCFs was a well-established, and thus it was easy to avoid the release of CoO NPs back into the water. In addition to this, WP-α-CFs loading with CoO NPs was favored by magnetite modification, suggests dual functionality of the developed bioadsorbent. Magnetic separation rate M-WP-αCFs was not reduced to a significant extent after deposition of CoO NPs on the exterior of the WP-αCFs, since robust bonding of Fe_3O_4 NPs,

which were formed through hydrogen bonding. Moreover, the M-WP-αCF-CoO NPs could be easily separated and recycled for fruther use from the reaction solution using magnetic force applied externally. Theses results show that the α-CFs from WP modified with Fe_3O_4 possess good supermagnetism. Such remediation products were separated from the reaction mixture; thus can be avoided to form secondary waste called sludge inherently hazardous, and used further for characterization and use.

3.6.3 TEM analysis

TEM analysis after the CoO NPs loading was also performed to reveal structural observations, elemental mapping, and EDS measurements (as shown in the supplementary material). TEM image of the CoO NPs showed a spindle, cuboidal and spherical shaped NPs with an average range of 10-20 nm were observed. TEM images of the M-WP-αCFs represented a CoO NPs loaded on the M-WP-αCFs surface. Very dense loading of CoO NPs onto M-WP-αCFs corroborated the obtained higher adsorption efficiency. The zoomed view of the TEM image of M-WP-αCF-CoO gave evidence of CoO NPs loading onto M-WP-αCFs surface. Furthermore, the very close look at the loaded CoO NPs from M-WP-αCF-CoO has revealed a typical lattice fringe regions of pure crystalline nature. The selected area electron diffraction (SAED) pattern of M-WP-αCF-CoO resembling the clear rings gave pure poly-crystalline nature of the loaded CoO NPs and Fe_3O_4 NPs. Moreover, the quantitative analysis of respective surface elements of M-WP-αCF-CoO was also made by TEM and EDS analysis. It showed a 92% (wt) of the surface cobalt element concentration. While, the surface concentration of Fe and C were observed to be 5.95 and 1.21 weight %, respectively. These all observed TEM results very strongly evidenced successful and high-capacity remediation of CoO NPs obtained by the

developed low-cost, rapidly-separable and inexpensive nano-composite of M-WP-αCFs. Since the WP-α-CFs surface has both CoO NPs and Fe_3O_4 NPs; visual mapping was needed to clear the presence and distribution of each particle. Therefore, high-angle annular dark-field scanning transmission electron microscopy (HAADF-STEM) was performed an elemental mapping from M-WP-αCF-CoO NPs. The obtained results were displayed in the supplementary material. The M-WP-αCF-CoO NPs surface was shown the distribution of C, Fe, and Co. (see in the supplementary material). Very dense distribution of Co was observed all over the surface of M-WP-αCFs. The obtained results visually confirmed the successful modification of WP-αCFs surface with the Fe_3O_4 NPs and further application of the M-WP-αCFs for successful higher-capacity remediation of CoO NPs from the water.

4. Conclusions

In summary, M-WP-αCFs was prepared, characterized, and applied for adsorptive-remediation of CoO NPs from the water. Adsorption kinetics followed a pseudo-second-order phenomenon. Langmuir adsorption isotherm model was best fit to the experimental data. RL factor values indicated favorable adsorption process. Effective adsorption of CoO NPs onto M-WP-αCF surfaces was verified by XPS, VSM, TEM, and EDS mapping. The derived bioadsorbent from the waste-biomass was desirable for CoO NPs remediation and rapidly-separable that avoids generation of hazardous secondary waste and sludge. Nevertheless, in keeping with the adsorption potential of the M-WP-αCFs, it can be explored for different nano-waste released into water.

Appendix A. Supplementary materials

E-supplementary data for this work can be found in e-version of this paper online

Acknowledgments

National Research Foundation South Korea supported this research under the Project No. 2017R1C1B-5017360. This work is also supported by a grant (2017001970003) from the Ministry of Environment, South Korea. This research work was endorsed by Dongguk University-Seoul, South Korea Research Fund 2017-2019.

Conflict of author

Authors declared the no conflict of author

References

1. Abidi, N., Cabrales, L., Haigler, C.H. 2014. Changes in the cell wall and cellulose content of developing cotton fibers investigated by FTIR spectroscopy. *Carbohydrate Polymers*, **100**, 9-16.
2. Bajpai, P. 2014. 1 - Introduction some excerpts taken from bajpai pratima, ‘advances in recycling and deinking’ 2006 with kind permission from pira international UK. *Recycling and Deinking of Recovered Paper*, (Ed.) P. Bajpai, Elsevier. Oxford, 1-19.

3. Balmuri, S.R., Selvaraj, U., Kumar, V.V., Anthony, S.P., Tsatsakis, A.M., Golokhvast, K.S., Raman, T. 2017. Effect of surfactant in mitigating cadmium oxide NPs toxicity: Implications for mitigating cadmium toxicity in environment. *Environmental Research*, **152**, 141-149.
4. Banza, C.L.N., Nawrot, T.S., Haufroid, V., Decrée, S., De Putter, T., Smolders, E., Kabyla, B.I., Luboya, O.N., Ilunga, A.N., Mutombo, A.M., Nemery, B. 2009. High human exposure to cobalt and other metals in Katanga, a mining area of the Democratic Republic of Congo. *Environmental Research*, **109**(6), 745-752.
5. Batley, G.E., Kirby, J.K., McLaughlin, M.J. 2013. Fate and Risks of Nanomaterials in Aquatic and Terrestrial Environments. *Accounts of Chemical Research*, **46**(3), 854-862.
6. Cai, Y., Yuan, F., Wang, X., Sun, Z., Chen, Y., Liu, Z., Wang, X., Yang, S., Wang, S. 2017. Synthesis of core–shell structured Fe_3O_4@carboxymethyl cellulose magnetic composite for highly efficient removal of Eu(III). *Cellulose*, **24**(1), 175-190.
7. Chen, H.-W., Chiang, Y.-D., Kung, C.-W., Sakai, N., Ikegami, M., Yamauchi, Y., Wu, K.C.W., Miyasaka, T., Ho, K.-C. 2014. Highly efficient plastic-based quasi-solid-state dye-sensitized solar cells with light-harvesting mesoporous silica nanoparticles gel-electrolyte. *Journal of Power Sources*, **245**, 411-417.
8. Dutta, S., Kim, J., Ide, Y., Ho Kim, J., Hossain, M.S.A., Bando, Y., Yamauchi, Y., Wu, K.C.W. 2017. 3D network of cellulose-based energy storage devices and related emerging applications. *Materials Horizons*, **4**(4), 522-545.
9. Faisal, M., Saquib, Q., Alatar, A.A., Al-Khedhairy, A.A., Ahmed, M., Ansari, S.M., Alwathnani, H.A., Dwivedi, S., Musarrat, J., Praveen, S. 2016. Cobalt oxide

nanoparticles aggravate DNA damage and cell death in eggplant via mitochondrial swelling and NO signaling pathway. *Biological Research*, **49**, 20.

10. Fang, S., Gu, W., Chen, L., Yu, Z., Dai, M., Lin, Y., Liao, Y., Ma, X. 2018. Ultrasonic pretreatment effects on the co-pyrolysis of municipal solid waste and paper sludge through orthogonal test. *Bioresource Technology*, **258**, 5-11.
11. Ghodake, G., Seo, Y.D., Lee, D.S. 2011. Hazardous phytotoxic nature of cobalt and zinc oxide nanoparticles assessed using *Allium cepa*. *Journal of Hazardous Materials*, **186**(1), 952-955.
12. Ghodake, G.S., Yang, J., Shinde, S.S., Mistry, B.M., Kim, D.-Y., Sung, J.-S., Kadam, A.A. 2018. Paper waste extracted α-cellulose fibers super-magnetized and chitosan-functionalized for covalent laccase immobilization. *Bioresource Technology*, **261**, 420-427.
13. Gomes, D.G., Serna-Loaiza, S., Cardona, C.A., Gama, M., Domingues, L. 2018. Insights into the economic viability of cellulases recycling on bioethanol production from recycled paper sludge. *Bioresource Technology*, **267**, 347-355.
14. Guacci, U., Traina, F., Ferraris, G.B., Barisone, R. 1977. On the application of the temkin equation in the evaluation of catalysts for the ammonia synthesis. *Industrial & Engineering Chemistry Process Design and Development*, **16**(2), 166-176.
15. Hutchison, J.E. 2016. The road to sustainable nanotechnology: challenges, progress and opportunities. *ACS Sustainable Chemistry & Engineering*, **4**(11), 5907-5914.
16. Kadam, A.A., Jang, J., Lee, D.S. 2016. Facile synthesis of pectin-stabilized magnetic graphene oxide Prussian blue nanocomposites for selective cesium removal from aqueous solution. *Bioresource Technology*, **216**, 391-398.

17. Kadam, A.A., Jang, J., Lee, D.S. 2017. Supermagnetically tuned halloysite nanotubes functionalized with aminosilane for covalent laccase immobilization. *ACS Applied Materials & Interfaces*, **9**(18), 15492-15501.

18. Kadam, A.A., Kamatkar, J.D., Khandare, R.V., Jadhav, J.P., Govindwar, S.P. 2013a. Solid-state fermentation: tool for bioremediation of adsorbed textile dyestuff on distillery industry waste-yeast biomass using isolated *Bacillus cereus* strain EBT1. *Environmental Science and Pollution Research*, **20**(2), 1009-1020.

19. Kadam, A.A., Lade, H.S., Patil, S.M., Govindwar, S.P. 2013b. Low cost $CaCl_2$ pretreatment of sugarcane bagasse for enhancement of textile dyes adsorption and subsequent biodegradation of adsorbed dyes under solid state fermentation. *Bioresource Technology*, **132**, 276-284.

20. Kadam, A.A., Lee, D.S. 2015. Glutaraldehyde cross-linked magnetic chitosan nanocomposites: Reduction precipitation synthesis, characterization, and application for removal of hazardous textile dyes. *Bioresource Technology*, **193**, 563-567.

21. Kazuhiko, M., Koki, I., Yuki, T., Daling, L., Miharu, E. 2016. Modification of wide-band-gap oxide semiconductors with cobalt hydroxide nanoclusters for visible-light water oxidation. *Angewandte Chemie International Edition*, **55**(29), 8309-8313.

22. Langmuir, I. 1916. The constitution and fundamental properties of solids and liquids. part I. solids. *Journal of the American Chemical Society*, **38**(11), 2221-2295.

23. LeVan, M.D., Vermeulen, T. 1981. Binary Langmuir and Freundlich isotherms for ideal adsorbed solutions. *The Journal of Physical Chemistry*, **85**(22), 3247-3250.

24. Loader, N.J., Robertson, I., Barker, A.C., Switsur, V.R., Waterhouse, J.S. 1997. An improved technique for the batch processing of small wholewood samples to α-cellulose. *Chemical Geology*, **136**(3), 313-317.

25. Ma, M.-G., Zhu, J.-F., Li, S.-M., Jia, N., Sun, R.-C. 2012. Nanocomposites of cellulose/iron oxide: influence of synthesis conditions on their morphological behavior and thermal stability. *Materials Science and Engineering: C*, **32**(6), 1511-1517.

26. Mukhopadhyay, A., Joshi, N., Chattopadhyay, K., De, G. 2012. A Facile synthesis of peg-coated magnetite (fe3o4) nanoparticles and their prevention of the reduction of cytochrome C. *ACS Applied Materials & Interfaces*, **4**(1), 142-149.

27. Nechyporchuk, O., Yu, J., Nierstrasz, V.A., Bordes, R. 2017. Cellulose nanofibril-based coatings of woven cotton fabrics for improved inkjet printing with a potential in e-textile manufacturing. *ACS Sustainable Chemistry & Engineering*, **5**(6), 4793-4801.

28. Nguyen, C.V., Liao, Y.-T., Kang, T.-C., Chen, J.E., Yoshikawa, T., Nakasaka, Y., Masuda, T., Wu, K.C.W. 2016. A metal-free, high nitrogen-doped nanoporous graphitic carbon catalyst for an effective aerobic HMF-to-FDCA conversion. *Green Chemistry*, **18**(22), 5957-5961.

29. Nowack, B., Bucheli, T.D. 2007. Occurrence, behavior and effects of nanoparticles in the environment. *Environmental Pollution*, **150**(1), 5-22.

30. Park, S., Baker, J.O., Himmel, M.E., Parilla, P.A., Johnson, D.K. 2010. Cellulose crystallinity index: measurement techniques and their impact on interpreting cellulase performance. *Biotechnology for Biofuels*, **3**(1), 10.

31. Peng, S., Meng, H., Ouyang, Y., Chang, J. 2014. Nanoporous magnetic cellulose–chitosan composite microspheres: preparation, characterization, and application for Cu(II) adsorption. *Industrial & Engineering Chemistry Research*, **53**(6), 2106-2113.

32. Phinichka, N., Kaenthong, S. 2018. Regenerated cellulose from high alpha cellulose pulp of steam-exploded sugarcane bagasse. *Journal of Materials Research and Technology*, **7**(1), 55-65.

33. Pivnenko, K., Eriksson, E., Astrup, T.F. 2015. Waste paper for recycling: Overview and identification of potentially critical substances. *Waste Management*, **45**, 134-142.

34. Quoc Buu, N., Trong Hien, D., Hoai Chau, N., Xuan Tin, T., Tuong Van, N., Thuy Duong, K., Thi Ha, H. 2014. Effects of nanocrystalline powders (Fe, Co and Cu) on the germination, growth, crop yield and product quality of soybean (Vietnamese species DT-51). *Advances in Natural Sciences: Nanoscience and Nanotechnology*, **5**(1), 015016.

35. Reijnders, L. 2006. Cleaner nanotechnology and hazard reduction of manufactured nanoparticles. *Journal of Cleaner Production*, **14**(2), 124-133.

36. Rotaru, R., Savin, M., Tudorachi, N., Peptu, C., Samoila, P., Sacarescu, L., Harabagiu, V. 2018. Ferromagnetic iron oxide–cellulose nanocomposites prepared by ultrasonication. *Polymer Chemistry*, **9**(7), 860-868.

37. Shieh, F.-K., Hsiao, C.-T., Kao, H.-M., Sue, Y.-C., Lin, K.-W., Wu, C.-C., Chen, X.-H., Wan, L., Hsu, M.-H., Hwu, J.R., Tsung, C.-K., Wu, K.C.W. 2013. Size-adjustable annular ring-functionalized mesoporous silica as effective and selective adsorbents for heavy metal ions. *RSC Advances*, **3**(48), 25686-25689.

38. Shieh, F.-K., Wang, S.-C., Yen, C.-I., Wu, C.-C., Dutta, S., Chou, L.-Y., Morabito, J.V., Hu, P., Hsu, M.-H., Wu, K.C.W., Tsung, C.-K. 2015. Imparting functionality to

biocatalysts via embedding enzymes into nanoporous materials by a de novo approach: Size-Selective Sheltering of Catalase in Metal–Organic Framework Microcrystals. *Journal of the American Chemical Society*, **137**(13), 4276-4279.

39. Silva, V.A.J., Andrade, P.L., Silva, M.P.C., Bustamante D, A., De Los Santos Valladares, L., Albino Aguiar, J. 2013. Synthesis and characterization of Fe_3O_4 nanoparticles coated with fucan polysaccharides. *Journal of Magnetism and Magnetic Materials*, **343**, 138-143.
40. Singh, P.P., Ambika. 2018. 10 - Environmental remediation by nanoadsorbents-based polymer nanocomposite. in: *New Polymer Nanocomposites for Environmental Remediation*, (Eds.) C.M. Hussain, A.K. Mishra, Elsevier, pp. 223-241.
41. Takagi, H., Nakagaito, A.N., Bistamam, M.S.A. 2013. Extraction of cellulose nanofiber from waste papers and application to reinforcement in biodegradable composites. *Journal of Reinforced Plastics and Composites*, **32**(20), 1542-1546.
42. Wagner, S., Gondikas, A., Neubauer, E., Hofmann, T., von der Kammer, F. 2014. Spot the difference: engineered and natural nanoparticles in the environment-release, behavior, and fate. *Angewandte Chemie International Edition*, **53**(46), 12398-12419.
43. Wahajuddin, Arora, S. 2012. Superparamagnetic iron oxide nanoparticles: magnetic nanoplatforms as drug carriers. *International Journal of Nanomedicine*, **7**, 3445-3471.
44. Wang, S., Lu, A., Zhang, L. 2016. Recent advances in regenerated cellulose materials. *Progress in Polymer Science*, **53**, 169-206.
45. Wiesner, M.R., Lowry, G.V., Alvarez, P., Dionysiou, D., Biswas, P. 2006. Assessing the risks of manufactured nanomaterials. *Environmental Science & Technology*, **40**(14), 4336-4345.

46. Xiu, M., Stevanovic, S., Rahman, M.M., Pourkhesalian, A.M., Morawska, L., Thai, P.K. 2018. Emissions of particulate matter, carbon monoxide and nitrogen oxides from the residential burning of waste paper briquettes and other fuels. *Environmental Research*.

47. Xiuyan, G., Zhengwu, J., Haoxin, L., Wenting, L. 2015. Production of recycled cellulose fibers from waste paper via ultrasonic wave processing. *Journal of Applied Polymer Science*, **132**(19).

48. You, G., Wang, P., Hou, J., Wang, C., Miao, L., Xu, Y., Feng, T. 2018. Influence of CeO_2 nanoparticles on viscoelastic properties of sludge: Role of extracellular polymeric substances. *Environmental Research*, **167**, 34-41.

49. Zare, E.N., Motahari, A., Sillanpää, M. 2018. Nanoadsorbents based on conducting polymer nanocomposites with main focus on polyaniline and its derivatives for removal of heavy metal ions/dyes: A review. *Environmental Research*, **162**, 173-195.

50. Zhou, Y., Zhang, M., Hu, X., Wang, X., Niu, J., Ma, T. 2013. Adsorption of cationic dyes on a cellulose-based multicarboxyl adsorbent. *Journal of Chemical & Engineering Data*, **58**(2), 413-421.

Table 1. Adsorption kinetic parameters, constants and regression coefficient values for CoO NPs adsorption on the M-WP-αCFs.

Adsorption Kinetics	
Pseudo first order kinetic model	Pseudo second order kinetic model
q_{eexp}=573	q_{eexp} =573
q_{ecal}=502	q_{ecal} =548
k_1=0.673	k_2=0.0016
R^2=0.8649	R^2=0.9486

Table 2. Different adsorption isotherm models studied and their obtained parameter values.

Isotherm model	Parameters	Obtained values
Langmuir	q_m (mg/g)	1567
	K_a (L/mg)	0.0071
	R^2	0.9903
Freundlich	K_F (mg/g)	68.920
	n	2.086
	R^2	0.9773
Tempkin	b_T	3.110
	A_T	0.07323
	R^2	0.9876

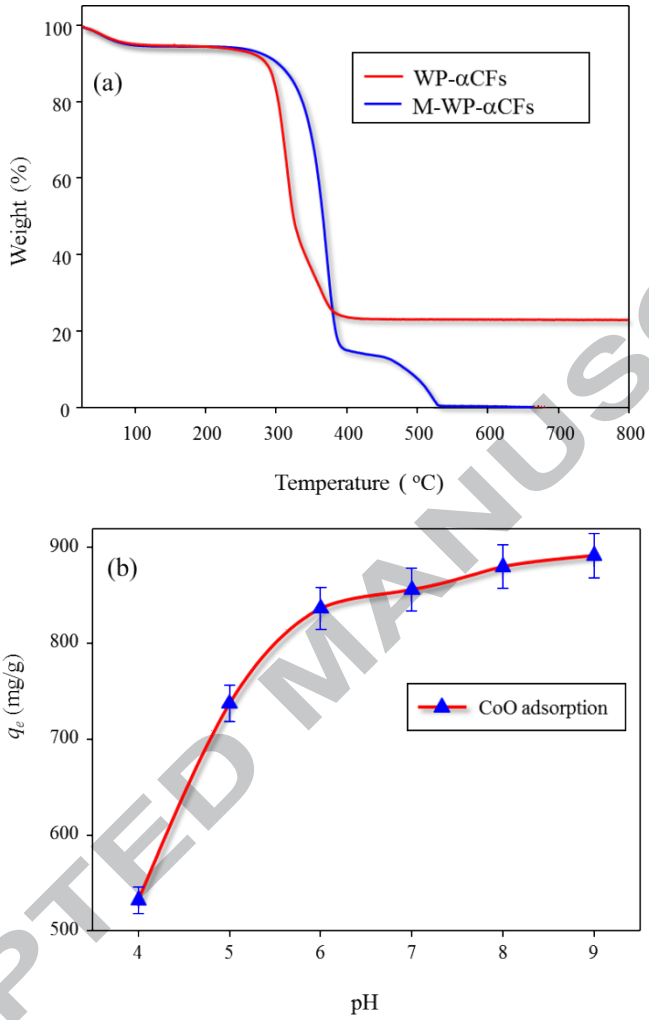

Fig. 1. (a) TGA pattern of WP-αCFs and M-WP-αCFs powder, and (b) effect of pH on adsorptive-removal of CoO (mg/g) by M-WP-αCFs.

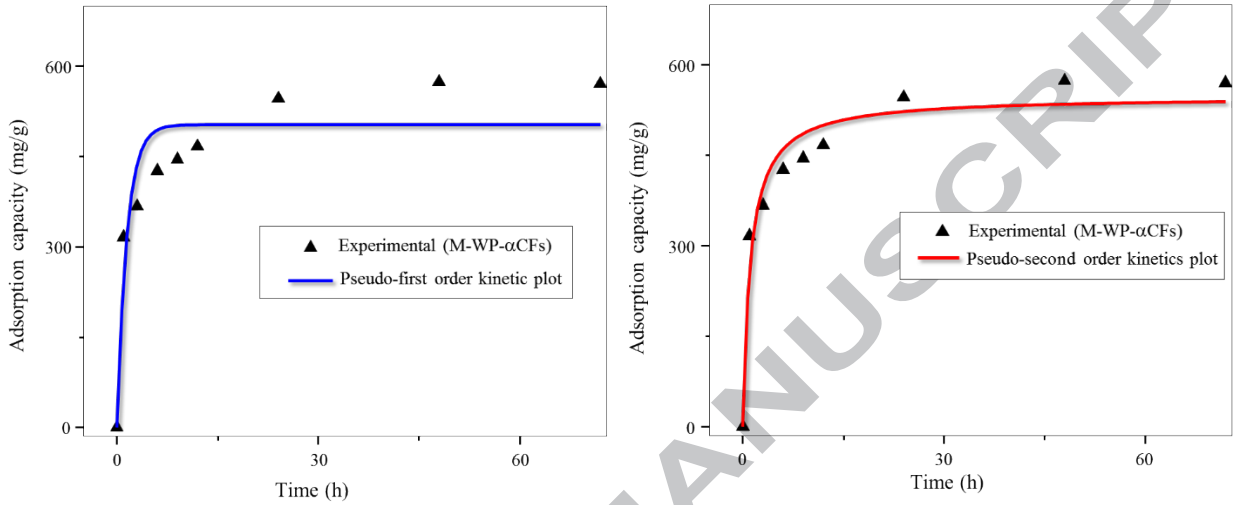

Fig. 2. (a) Pseudo-first order kinetic model for CoO adsorption on M-WP-αCFs (b) Pseudo-second order kinetic model for CoO adsorption on M-WP-αCFs.

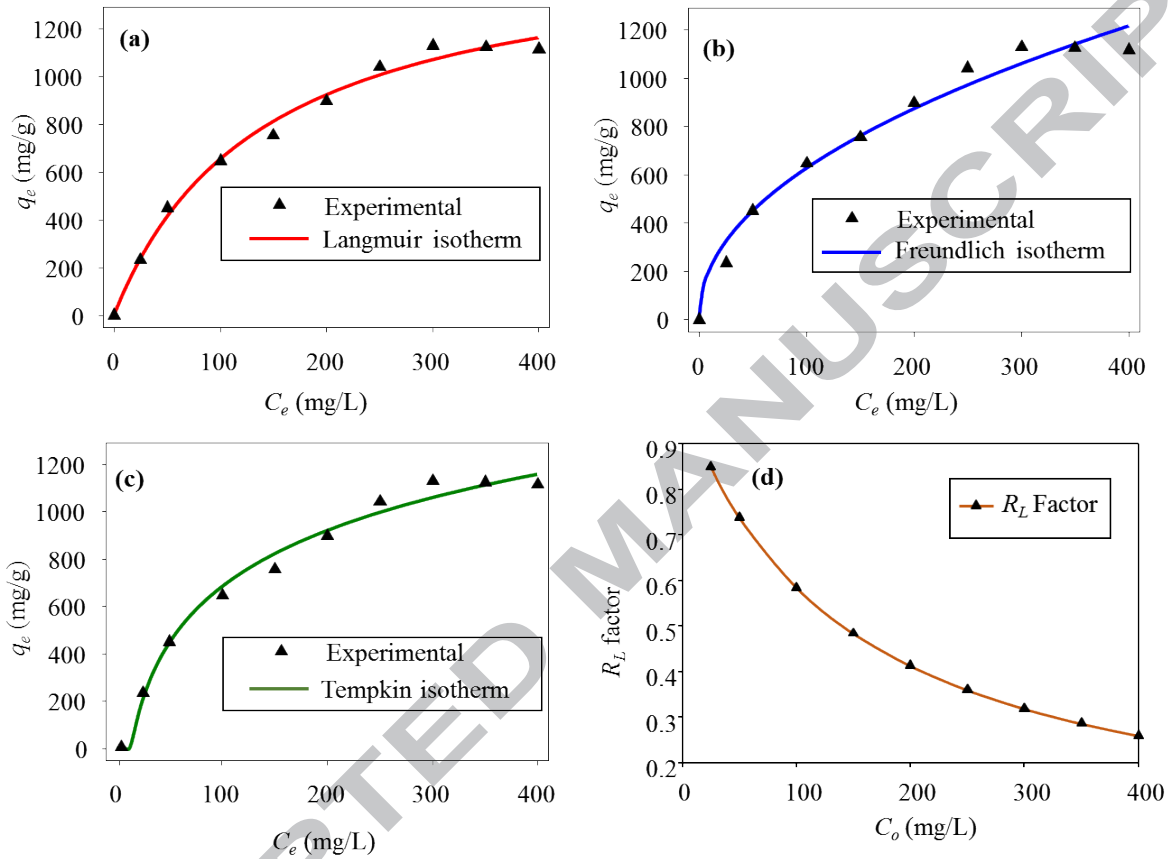

Fig. 3. Adsorption isotherms of CoO on M-WP-αCFs (a) Langmuir isotherm plot (b) Freundlich isotherm plot (c) Tempkin isotherm plot and (d) R_L factor values.

Graphical abstract

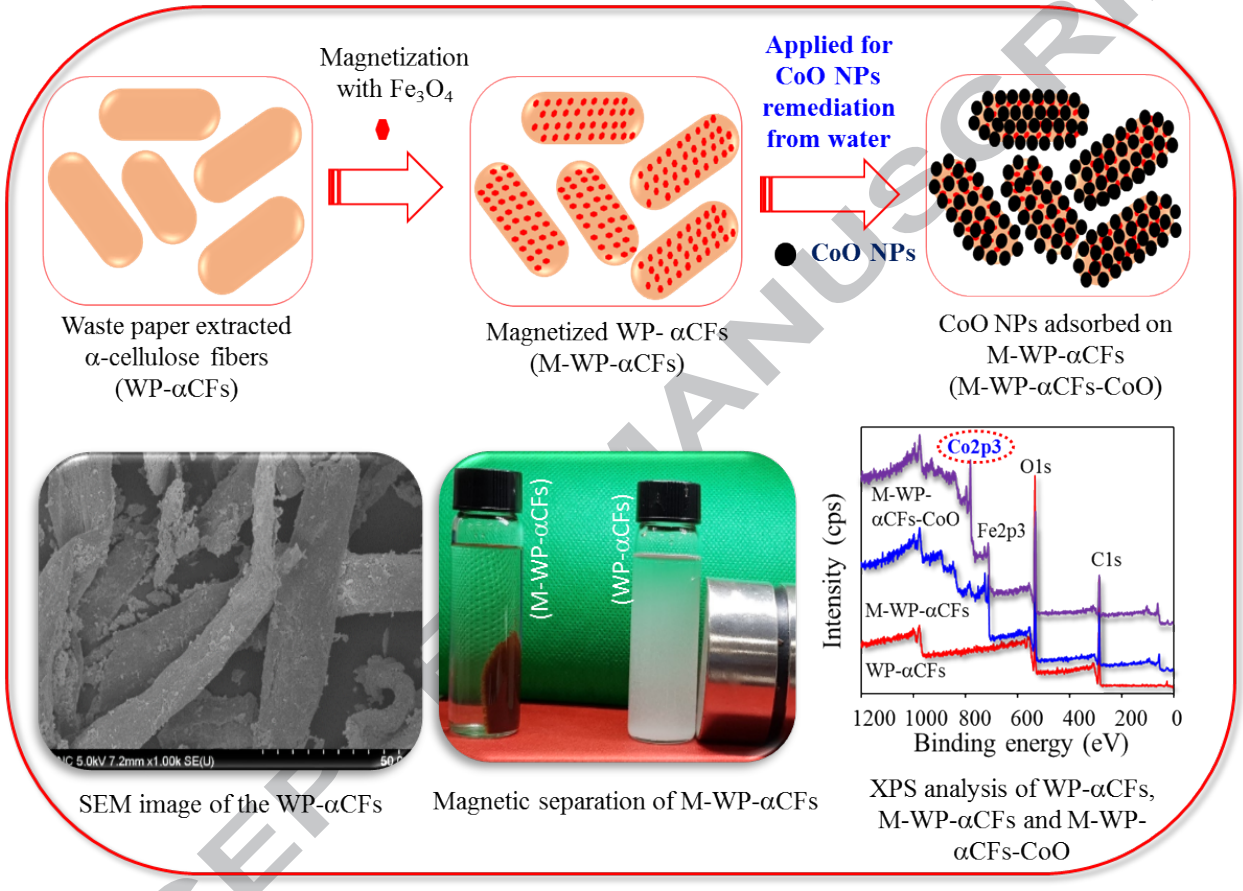

Research highlights

1. Office paper waste (WP) extracted α-cellulose fibers (αCFs) was magnetized
2. M-WP-αCFs presented an effective adsorptive-remediation of CoO NPs from the water
3. The adsorption kinetics followed a pseudo-second-order rate model
4. Langmuir adsorption isotherm model was best fit to the experimental data
5. M-WP-αCFs can be effective for remediation of engineered NPs from the water